

QCD phase diagram: Comparison between lattice and hadron resonance gas model results

K. Redlich*

Institute for Theoretical Physics, University of Wroclaw, Pl 45204 Wroclaw, Poland

A. Tawfik†

*Faculty for Physics, University of Bielefeld,
P.O. Box 100131, D-33501 Bielefeld, Germany*

(Dated: 2nd December 2024)

Abstract

We compare the lattice results on QCD phase diagram for two and three flavors with the hadron resonance gas model (HRGM). Lines of constant energy density ϵ have been determined at different chemical potentials μ . For the strangeness chemical potentials μ_S , we use two models. In the first one, we explicitly set $\mu_S = 0$ for all temperatures and baryo-chemical potentials μ_B . This condition is used in lattice QCD simulations. In the other model, μ_S is calculated in dependence on T and μ_B according to the condition of vanishing strangeness. Furthermore, with applying Taylor expansion, we derive an analytical expression for the dependence of T_c on μ/T . The HRGM results on $T_c - \mu$ phase diagram are compared with lattice QCD simulations for different flavors and quark masses. The agreement is excellent, especially when the trigonometric function in the expression of ϵ is truncated up to the same orders as in lattice QCD simulations. For studying the efficiency of the truncated Taylor series in describing the phase transition, we recall the radius of convergence. For zero- and second-order radii, the agreement is strong convincing.

PACS numbers:

*Electronic address: redlich@ift.uni.wroc.pl

†Electronic address: tawfik@physik.uni-bielefeld.de

I. INTRODUCTION

The QCD phase diagram at finite temperature and density attracted increasing attention [1], especially as it became possible to perform lattice QCD simulations at non-zero baryon number density μ_B [2–5]. The numerical studies of the equation of state at finite densities can provide a valuable framework for understanding the experimental signatures for the phase transition from the confined hadronic matter to the quark-gluon plasma (QGP). The heavy-ion collision experiments are aiming to explore the QCD phase diagram. Therefore, it is of great interest to show the interrelation between the baryon and strange quark chemical potentials and T_c in the hadron resonance gas model (HRGM) compared with the available lattice QCD simulations.

It is known that the QCD phase diagram has a very rich structure. From numerical simulations, we know that the location of the phase transition line depends on the quark masses, the number of flavors and the way of including the strange quark chemical potential μ_s at different values of μ_B and T . The isospin chemical potential can play an additional role. But relative to μ_B and μ_s , the isospin chemical potential is very small, so that we can assume an entire symmetry in the light quark potentials and therefore ignore the isospin chemical potential.

The first point in the QCD phase diagram, namely the point at T_c and $\mu = 0$, has been a subject of different lattice simulations [2–8]. We know so far that for two quark flavors ($n_f = 2$) the transition is second order or rapid crossover and the critical temperature is $T_c \approx 170$ MeV. For $n_f = 3$, we have a first order phase transition and $T_c \approx 155$ MeV. For $n_f = 2 + 1$, i.e. two degenerate light quarks and one heavy strange quark, the transition is crossover and $T_c \approx 170$ MeV. For the pure gauge theory, $T_c \approx 270$ MeV and the deconfinement phase transition is first order.

The lattice QCD simulations at $\mu_B \neq 0$ is still lacking an effective exact algorithm and suffer from the sign-problem. The fermion determinant gets complex and therefore the conventional Monte Carlo techniques are no longer applicable, since the lattice configurations can no longer be generated with the probability of the Boltzmann weight. However, during the last few years considerable progress has been made to overcome these problems [2–5, 9, 10].

The significant numerical results on positioning the QCD phase diagram we have so far is that the transition line can be described by a parabola. The parabola can be viewed as a reflection of the truncations done in the Taylor expansions of the thermodynamic quantities calculated on lattice. In addition, we know from many effective models such as thermal, bootstrap and Nambu-Jona-Lasinio models that the structure of the phase diagram is complex. Furthermore, the freeze-out curve takes a much different behavior at large chemical potential [11, 12]. Nevertheless, one might think that for small chemical potential ($\mu_q \approx T_c$) the curvature in the T_c -dependence on μ_q could be fitted as a parabola, where μ_q is the quark baryo-chemical potential. The situation for large chemical potentials is not yet clear. One might need to take into account other effects, such as quantum effects at low temperatures [13–18], which might be able to describe the change in the correlations from confined hadrons to coupled quark-pairs.

In the present work, we take advantage of our previous work [19–21] on analysis the critical temperatures T_c for different quark masses and on reproducing the lattice thermodynamics at zero and finite μ by means of HRGM. The deconfinement is driven by a constant energy density. We have shown [19, 20] that the degrees of freedom rapidly increase at $\epsilon_c(T_c, \mu = 0)$. In present work, we assume that $\epsilon_c(T_c, \mu = 0)$ remains constant along the whole phase transition line [21, 22]. Concretely, we propose that the existence of different transitions does not affect our assumption that ϵ_c is constant for all μ -values. We have to emphasize here that it is not possible in the framework of this model to make any statement about the transition at very high μ and low T . The nature of the degrees of freedom in this region is very different from that of the *nearly* non-interacting QGP at high T and low μ . The message is that the condition driving the QCD phase transition at finite T and μ [19–21] is the energy density. Its value is not affected by the conjecture of existing of different transitions along the whole μ -axis.

II. THE MODEL

Assuming an ideal quantum gas consisting of point-like hadron resonances, the canonical partition function for one resonance particle and its anti-particle reads

$$\mathcal{Z}(V, T, \mu) = g \frac{V}{2\pi^2} \int_0^\infty dk \, k^2 \left\{ \ln(1 \pm e^{-(\varepsilon - \mu)/T}) + \ln(1 \pm e^{-(\varepsilon + \mu)/T}) \right\}, \quad (1)$$

where \pm stand for bosons and fermions, respectively. $\varepsilon = (k^2 + m^2)^{1/2}$ is the single-particle energy and g is the spin-isospin degeneracy factor. Under the given assumptions, one can sum up the contributions from all resonances pieces, so that

$$\ln \mathcal{Z}^{(id)}(V, T, \mu) = \sum_i^\infty \ln \mathcal{Z}_i(V, T, \mu_i). \quad (2)$$

In this expression, there are important features included; the kinetic energies and the summation over all degrees of freedom and energy variables from the hadron resonances. On the other hand, the formation of resonances can only be materialized through strong interactions [23]; *Resonances (fireballs) are composed of further resonances (fireballs), which in turn consist of resonances (fireballs) and so on.*

In spite of this, if one would like to take into consideration all kinds of interactions between the resonances, then, for instance, by means of the S -matrix, we can re-write Eq. (2) as an expansion of the fugacity term. The S -matrix describes the scattering processes in the thermodynamical system [24].

$$\ln \mathcal{Z}^{(int)}(V, T, \mu) = \ln \mathcal{Z}^{(id)}(V, T, \mu) + \sum_{\nu=2}^\infty a_\nu(T) \exp(\mu_\nu/T). \quad (3)$$

Here, $a_\nu(T)$ are the so-called virial coefficients and the subscript ν refers to the order of the multiple-particle interactions,

$$a_\nu(T) = \frac{g_r}{2\pi^3} \int_{M_\nu}^\infty dw \, e^{-\varepsilon_r(w)/T} \sum_l (2l+1) \frac{\partial}{\partial w} \delta_l(w). \quad (4)$$

The sum runs over the spatial waves. The phase shift $\delta_l(w)$ of two-body inelastic interactions, for instance, depends on the resonance half-width Γ_r , spin and mass of the resulting resonance particles,

$$\ln \mathcal{Z}^{(int)}(V, T, \mu) = \ln \mathcal{Z}^{(id)}(V, T, \mu) + \frac{g_r}{2\pi^3} \int_{M_\nu}^\infty dw \frac{\Gamma_r e^{(-\varepsilon_r(w)+\mu_r)/T}}{(M_r - w)^2 + \left(\frac{\Gamma_r}{2}\right)^2}. \quad (5)$$

By inserting $-\mu$ in place of μ in Eq. (5), we take into consideration the two-particle inelastic interactions, from which the anti-particles will be produced. For narrow width and/or

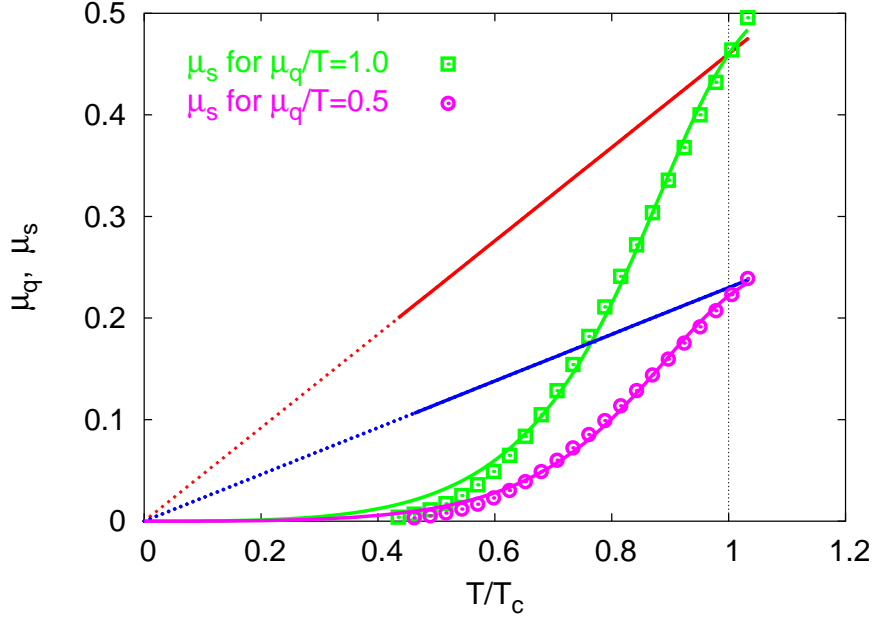


Fig. 1: The strange quark chemical potential μ_s vs. T/T_c for $\mu_q/T = 1$ and $\mu_q/T = 0.5$ (straight lines). The results are fitted according to Eq. (9). At $T = 0$, we find that $\mu_q = \mu_s = 0$. As $T \rightarrow T_c$, the strangeness chemical potential approaches the baryo-chemical potential, $\mu_s = \mu_q$. The units used here are $\sqrt{\sigma} \sim 420$ MeV.

at low temperatures the virial term reduces, so that we will get the *non-relativistic* ideal partition function of the hadron resonances with effective masses M_ν . In other words, the resonance contributions to the partition function are the same as that of free particles with some effective mass. At temperatures comparable to Γ_r , the effective mass approaches the physical one measured in the vacuum. **Thus, at high temperatures, the strong interactions are taken into consideration via including the hadron resonances as done in Eq. (2).** We therefore suggest to use the canonical partition function Eq. (2) without any corrections. Furthermore, we do not apply corrections due to the excluded volume. We include all hadron resonances with masses up to 2 GeV, such a way we avoid the singularities expected for heavy resonances at the Hagedorn temperature [19, 20].

In the two sections which follow, we discuss how to include the strangeness chemical potential μ_s in HRGM and lattice QCD.

A. μ_s in hadron resonance gas model

The *hadron*-based chemical potentials μ_B, μ_S is related to the *quark*-based ones, μ_q, μ_s

$$\mu_B = 3\mu_q, \quad \mu_S = \mu_q - \mu_s, \quad (6)$$

Assuming the isospin and charge chemical potentials are vanishing, we use the following combination for hadron resonances

$$\mu = 3b\mu_q + s\mu_s, \quad (7)$$

where b and s are the baryon and strange quantum numbers, respectively. The quantum numbers are conserved in these expressions.

Apparently, the initial conditions in heavy-ion collisions include zero net strangeness. This is expected to remain the case during the whole interaction unless an asymmetry in the production of strange particles happens during the hadronization, the transition from QGP to hadrons. As we are interested in the thermodynamics in the hadronic matter and the location of the phase transition line, we suppose that the net strangeness is entirely vanishing. The average strange particle number is

$$\langle n_s \rangle = \frac{1}{N} \sum_i^N \lambda_s^{(i)} \frac{\partial \ln \mathcal{Z}^{(i)}(V, T, \mu)}{\partial \lambda_s^{(i)}}. \quad (8)$$

$\ln \mathcal{Z}$ is given in Eq. (3) and μ_S is given in Eq. (6). $\lambda_s = \exp(\mu_S/T)$ is the fugacity factor of s quark. The procedure used to calculate the *quark*-based μ_s is the following: For given T and μ_q (or μ_B), we iteratively increase μ_s starting from zero. In each iteration, we calculate the difference $\langle n_s \rangle - \langle n_{\bar{s}} \rangle$ via Eq. (8). The value of μ_s which leads to zero net strangeness is the one we read out and shall use in calculating the thermodynamic quantities. As in Eq. (8) the relation between μ_s and μ_S is given by taking into consideration the baryonic property of s -quark. The resulting μ_s for different μ_q (or μ_B) and T are depicted in Fig. 1. From this *numerical* method, we can fit μ_s as a function of T and μ_B ,

$$\mu_s \approx \frac{0.138 \vartheta \theta^3}{1 - 2.4 \theta^2 + 2.7 \theta^3}, \quad (9)$$

where $\vartheta \equiv \mu_q/T$ and $\theta \equiv T/T_c$.

Let us note here that for these calculations we have *re-scaled* the resonance masses in order to be comparable to the quark (pion) masses used in lattice QCD simulations. The procedure of giving *unphysically* very heavy masses to the quarks and correspondingly to the hadron resonances is introduced in Ref. [19, 20]. In these calculations, the lightest Goldstone meson gets the mass $m_\pi = 770$ MeV and consequently, the critical temperature becomes almost as large as 200 MeV at zero chemical potential.

In order to guarantee vanishing net strange particle numbers in HRGM or other thermal models as the case in heavy-ion experiments, it is not enough to simply set $\mu_s = 0$ and consequently, $\mu_s = \mu_q = \mu_B/3$ in Eq. (8). However, there are publications in which the authors have assigned μ_s to zero in the hadron matter and afterwards applied the Gibbs condition for the (first order) phase transition to QGP. The reason is obvious. Aside the baryons, the strange mesons with different contents of s quarks play determining roles at different temperatures and therefore, affect the final results, Eq. (9). Setting $\mu_s = 0$, leads to violating the strange quantum number. Nevertheless, in order to extensively compare with lattice results, we will show calculations in which we set $\mu_s = 0$. In other words, we apply this assignment in order to show the ability of HRGM in reproducing the current lattice simulations [22]. After accomplishing this successfully, we can go beyond the lattice constraints to show the physical picture.

For completeness of the discussion, we recall the situation in the plasma regime (see also next section). For conserving strangeness at $T > T_c$, we can only suppose that $\mu_s = 0$. μ_s consists of a baryonic part $\mu_B/3$ and another part coming from the strange quantum number $-\mu_s$. From Eq. (9), we then get

$$\mu_s = \mu_q = \mu_B/3. \quad (10)$$

This result can be seen in Fig. 1. For $\mu_q = 0$ (or $\mu_B = 0$), we find that $\mu_s = 0$ for all temperatures. μ_s increases with increasing μ_q and T . The most significant result is that $\mu_q \approx \mu_s$ at T_c . Therefore, we can suggest to set $\mu_q = \mu_s$ for all temperatures above T_c .

We can so far summarize that μ_s in the hadron matter has to be calculated in dependence on μ_B and T under the assumption that the net strangeness is vanishing. In the QGP phase, the only way to fulfill this assumption is to assign $\mu_s = \mu_B/3$. As we will see later, in lattice QCD simulations $\mu_s = \mu_s = 0$. We deal with these cases in the present work.

B. μ_s in lattice QCD

In the Euclidian path integral formulation, the partition function of lattice QCD at finite temperature T and chemical potential μ (Eq. (7)) reads

$$\mathcal{Z}(T, \mu) = \text{Tr } e^{-(H-\mu N)/T} = \int \mathcal{D}\psi \mathcal{D}\bar{\psi} \mathcal{D}A e^{\mathcal{S}_f(V, T, \mu) + \mathcal{S}_g(V, T)}, \quad (11)$$

where $(\psi, \bar{\psi})$ and A are the fermion and gauge fields, respectively. By Legendre transformation of the Hamiltonian H , we get the Euclidian action $\mathcal{S} = \int_0^{1/T} dt \int_V d^3x \mathcal{L}$. The fermionic action is

$$\mathcal{S}_f = a^3 \sum_x \left[m a \bar{\psi}_x \psi_x + \frac{1}{2} \sum_{k=1}^4 (\bar{\psi}_x \gamma_k \psi_{x+k} - \bar{\psi}_{x+k} \gamma_k \psi_x) + \mu a \bar{\psi}_x \gamma_4 \psi_x \right], \quad (12)$$

where a is the lattice spacing. As given in Eq. (6), the number density of the quarks with flavor number x is obtained by the first derivative with respect to μ_x ,

$$n_x = \frac{\partial}{\partial \mu_x} \ln \mathcal{Z}(T, \mu_x). \quad (13)$$

For checking the dependence of μ_s on μ_q and consequently on μ_B , it is enough to approximate the fermionic part of lattice QCD Lagrangian with three quark flavors as

$$\mathcal{L} \approx \mu_q \left(\sum_{x \in \{u, d\}} \bar{\psi}_x \gamma_4 \psi_x \right) + \mu_s \bar{\psi}_s \gamma_4 \psi_s \approx \mu_q n_u + \mu_q n_d + \mu_s n_s. \quad (14)$$

In order to take into account the conservation of the baryon and strange quantum numbers, the summation in last expression has to run over s -quarks, too. Doing this, the last term turns to be $(\mu_q - \mu_s) n_s$. Then the strangeness entirely vanishes at $\mu_s = \mu_q$. From Eq. (14), $n_s = 0$ in lattice calculations at $\mu_s = 0$.

As discussed in the previous section, the strangeness in QGP is conserved for $\mu_s = \mu_q = \mu_B/3$. In the hadron regime, especially at large μ_B , μ_s (or μ_S) has to be calculated as a function of both T and μ_B (Fig. 1). In spite of these considerations, the reliable lattice QCD simulations are still limited to $\mu_B \approx 3T_c$. As we will see in Sec. V, at this small value of the baryo-chemical potential, there is practically no big difference between $\mu_s = 0$ and $\mu_s = f(T, \mu_B)$.

III. LINES OF CONSTANT T_c

A. $T_c(\mu)$ in hadron resonance gas model

In the Boltzmann limit, the energy density of a system consisting of one particle and its anti-particle can be expressed as

$$\epsilon(T, \mu) = \frac{g}{\pi^2} T m^2 \left[m K_1 \left(\frac{m}{T} \right) + 3 T K_2 \left(\frac{m}{T} \right) \right] \cosh \left(\frac{\mu}{T} \right). \quad (15)$$

μ is given in Eq. (7). According to the efficiency of the fugacity term, we can divide this expression into two sectors: one meson- m and one baryon-sector b [20, 25],

$$\varepsilon_h(T, \mu) = \varepsilon_m(T) + \varepsilon_b(T) \cosh(\mu/T). \quad (16)$$

Applying truncation in the Taylor expansion up to the second order in μ/T - as done in the lattice calculations [26] - we can estimate the lines of constant T_c in HRGM. In doing this, we assume that $\varepsilon_h(T, \mu) = \varepsilon_h(T_c, 0)$. We also assume that the dependence of the energy density on the quark mass is quite small. We see this in Fig. 2 which is reported in Ref. [27]. At T_c and for the same temporal lattice dimension N_τ , there is very small change in the value of ε_c for different quark masses. The latter are related to the pion masses via $m_\pi^2 \propto m_q$.

The starting point in expressing $T_c(\mu)$ for constant ratios μ/T is to expand the above Taylor series Eq. (16) up to the some orders around the points $T = T_c$ and $\mu = 0$. The second-order expansion gives

$$\begin{aligned} \varepsilon_h(T, \mu_B) &= \varepsilon_h(T_c, 0) + \left[\frac{\partial \varepsilon_h(T_c, 0)}{\partial T} (T - T_c) + \frac{1}{2} \mu_B^2 \frac{\partial^2 \varepsilon_b(T_c, 0)}{\partial \mu_B^2} \right], \\ &= \varepsilon_h(T_c, 0) + \left[\frac{\partial \varepsilon_h(T_c, 0)}{\partial T} (T - T_c) + \frac{1}{2} \varepsilon_b(T_c, 0) \left(\frac{\mu_B}{T} \right)^2 \right]. \end{aligned} \quad (17)$$

Under the assumptions given above, this leads to the following parabola:

$$\frac{T_c(\mu_B)}{T_c(\mu_B = 0)} = 1 - \frac{9}{2} \frac{1}{T_c(\mu_B = 0)} \left[\frac{\varepsilon_b(T_c, 0)}{\frac{\partial}{\partial T} \varepsilon_h(T_c, 0)} \right] \left(\frac{\mu_q}{T} \right)^2, \quad (18)$$

where $\mu_q = \mu_B/3$. In order to map out the QCD phase diagram by using this analytic expression, we merely need to calculate the baryon energy density ϵ_b at T_c and $\mu_q = 0$ and the derivative of the hadron energy density with respect to the temperature at the

same point. The results are given in Sec. V. Evidently, it is possible to extend the above expression to include further higher terms of μ_q/T .

Then to determine T_c at finite μ , we apply besides this analytical method the condition of constant critical energy density [21, 22] (see Sec. IV). T_c is defined as the temperature at which the energy density of hadron resonance gas reaches a certain critical value. Its value is to be taken from lattice QCD simulations at $\mu_B = 0$.

B. $T_c(\mu)$ in lattice QCD

In lattice QCD simulations, the critical temperature $T_c(\mu)$ is to be calculated from the pseudo-critical coupling $\beta_c(\mu)$ by determining the susceptibility peak in either the Polyakov loop or the chiral condensate in $\beta - \mu$ dimensions. The lattice beta function $\beta(a)$ which can be obtained from the string tension is needed in order to express the results in physical units. From the first non-trivial Taylor coefficients of $T_c(\mu)$, we get

$$\frac{d^2}{d\mu^2} T_c(\mu) = -\frac{N_\tau^{-2}}{T_c(\mu=0)} \frac{\partial^2 \beta_c(\mu)}{\partial \mu^2} \left(a^{-1} \frac{\partial a}{\partial \beta} \right), \quad (19)$$

where N_τ is the temporal lattice dimension.

In the lattice QCD simulations [4] with $n_f = 2$ and quark mass $am_q = 0.1$, the dependence of T_c on μ_q has been found to take the following expression (parabola):

$$\frac{T_c(\mu_q)}{T_c(\mu_q=0)} = 1 - 0.070(35) \left(\frac{\mu_q}{T_c(\mu_q=0)} \right)^2. \quad (20)$$

In other lattice QCD simulations with the same flavor number but with quark masses four times heavier than their physical masses [3], it has been found that the parabola (curvature) takes the following form:

$$\frac{T_c(\mu_q)}{T_c(\mu_q=0)} = 1 - 0.050(34) \left(\frac{\mu_q}{T_c(\mu_q=0)} \right)^2. \quad (21)$$

In Ref. [4], it has been concluded that the last relation remains almost unchanged for much small quark mass $am_q = 0.005$. In this regard, we have to remember that for small quark masses the perturbative beta function has been used. As we will see later, we actually find an increase in the curvature with reducing the resonance masses from the values which very well simulate the current lattice calculations ($m_\pi \approx 770$ MeV) to the physical masses, at which the lightest Goldstone meson mass is $m_\pi = 140$ MeV.

The results from Eq. (20) are depicted in Fig. 3. In the same figure, we draw Eq. (21). We show other lattice results, namely the short vertical lines which draw the lattice results [4] on T_c corresponding to a constant energy density.

The $n_f = 3$ lattice QCD results [28] for different quark masses obtained so far can be summarized as

$$\frac{T_c(\mu_q)}{T_c(\mu_q = 0)} = 1 - 0.025(6) \left(\frac{\mu_q}{T_c(\mu_q = 0)} \right)^2, \quad am_q = 0.1, \quad (22)$$

$$= 1 - 0.114(46) \left(\frac{\mu_q}{T_c(\mu_q = 0)} \right)^2, \quad am_q = 0.005. \quad (23)$$

Again, in these simulations the beta function for the small quark masses has been calculated perturbatively. The results from these two expressions are depicted in Fig. 5 and Fig. 6, respectively. In other $n_f = 3$ lattice QCD simulations [29], it is found that $T_c(\mu_q \neq 0)$ takes the following expression:

$$\frac{T_c(\mu_q)}{T_c(\mu_q = 0)} = 1 - 0.0610(90) \left(\frac{\mu_q}{T} \right)^2 + 0.00235(89) \left(\frac{\mu_q}{T} \right)^4. \quad (24)$$

The curvature from the $2+1$ lattice simulations [30] has been compared with the three flavor one [3] and concluded that there is a complete agreement. As we will see in Fig. 6, the most recent $2+1$ lattice simulations [31] results in a curvature that is much smaller than those from other lattice simulations. This can be understood according to the different actions.

IV. LINES OF CONSTANT ENERGY DENSITY

In previous work [21], we used HRGM in order to determine T_c corresponding to a wide range of quark (pion) masses at vanishing chemical potential μ . The masses range from the chiral up to the pure gauge limits. We have seen that the condition of a constant energy density can excellently reproduce the critical temperature T_c as a function of both quark mass m_q and flavor number n_f . In the present work, we extend this condition to finite chemical potentials. We use two models for including the strangeness chemical potential μ_S . In the first model, we calculate μ_S in dependence on μ_B and T according to the condition of zero net strangeness. In the other one, we explicitly set the quark-based $\mu_s = 0$. The latter case is usually being used in lattice QCD simulations. As given in Sec. II B, the proper

inclusion of μ_s in QGP and in the Lagrangian of lattice QCD is to assign to it the same value of $\mu_B/3$. Nevertheless, both choices can be accepted for the current lattice QCD simulations. The most reliable lattice calculations are performed at small baryo-chemical potentials. i.e. of the order of T_c ($\mu_q \approx T$). Consequently, the strangeness chemical potential will be small too.

As discussed above, in HRGM, the energy density at finite chemical potential can be divided into two parts: one from the meson sector and another one from the baryon sector. For the first part, we can completely drop out the fugacity term, especially for the chemical potentials of light quarks. For symmetric numbers of light quarks, the baryo-chemical potential of the mesons is vanishing. But for the strange mesons the strangeness chemical potential assigned to their strange quark content should be taken into account. For the baryon sector, Eq. (6) have to be applied.

The question we intent to answer is: which value has to be assigned to the critical energy density? We recall the lattice QCD simulations. In Fig. 2, we see that the energy density [33] at the corresponding T_c is not a singular function but can rather be defined at different *critical* values depending on the flavor number and quark mass. The uncertainty in the energy density is therefore large. The critical energy density at which we define our critical temperatures $T_c(\mu)$ is taken from the lattice QCD simulations at $\mu_B = 0$ [8]. In lattice units, the dimensionless energy density for $n_f = 2$ and 3 are $\varepsilon/T^4|_{T_c} \cong 4.5 \pm 2$ and $\cong 6.5 \pm 2$, respectively. We drop out the errors in these quantities. We take an average value and recalculate it in the physical units. Then, $\epsilon_c = 600 \pm 300$ MeV/fm³. It is assumed that this value is independent on the quark masses and remains constant on the whole μ -axis.

V. THE RESULTS

Since we intend to compare HRGM with lattice results [3, 4], some details about the lattice QCD simulations at $\mu_q \neq 0$ are in order. On the other hand, details about HRGM are partially given in the present work. The whole details are introduced in Refs. [19–21]. In order to avoid the sign problem in lattice QCD simulations, two related steps are done in Ref. [4]. The derivatives of the thermodynamic quantities with respect to $\mu_B = 0$ at the point T_c are first computed and then their Taylor expansion coefficients in terms of finite μ_q

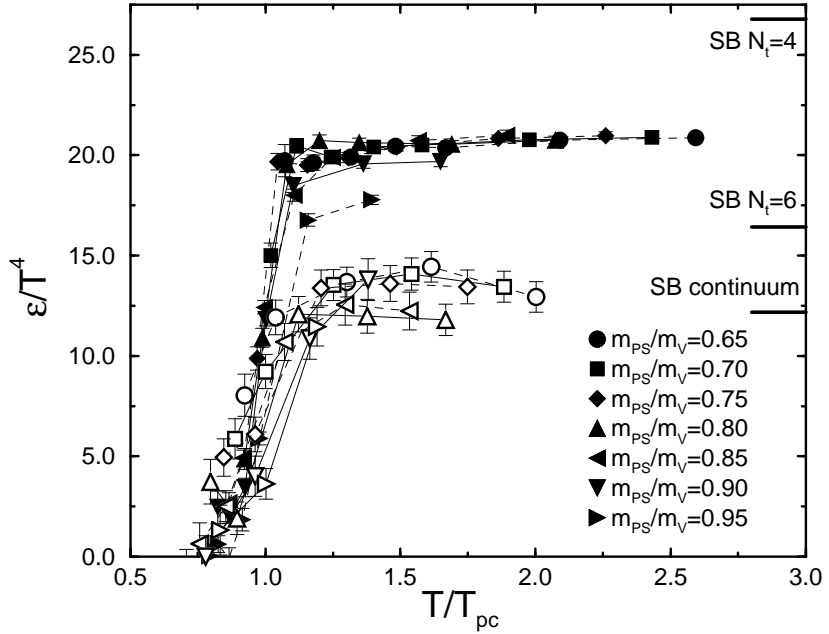


Fig. 2: The energy density normalized to T^4 given in dependence on T/T_c for different quark masses m_q and temporal lattice dimensions N_τ . This figure is reported in Ref. [27].

are calculated. The curvatures drawn by $T_c(\mu_B)$ and $\epsilon_c(\mu_B)$ are derived for different quark masses. For instance for $am_q = 0.1$, the corresponding pion mass in lattice units for $n_f = 2$ is $am_\pi = 0.958(2)$, where $a\sigma = 0.271(10)$ [8]. This leads to $m_\pi \cong 773$ MeV. Keeping these features in mind, we performed our calculations for physical and re-scaled masses of the hadron resonances. In Fig. 3, we see that our results coincide very well with the lattice results. In Ref. [3], lattice QCD simulations are performed with an imaginary chemical potential for the two flavors of the staggered quarks. For $\mu = i\mu_I$, the sign problem is no longer existing. Using analytic continuation of the truncated Taylor series, one can then go to real μ . The light quark mass is four times heavier than its physical mass. The location of T_c at $\mu_B = 0$ has been extrapolated to the chiral limit. The simulations are represented by the short curves in Figs. 3, 4 and 6.

A. Results for two flavors

From the canonical partition function Eq. (1), we can derive the energy density at finite chemical potential $\mu \neq 0$ as

$$\epsilon(T, \mu) = T \frac{\partial T \ln \mathcal{Z}(T, \mu)}{\partial T} - T \ln \mathcal{Z}(T, \mu) + \mu \frac{\partial T \ln \mathcal{Z}(T, \mu)}{\partial \mu} = \frac{g}{2\pi^2} \int_0^\infty k^2 dk \frac{\varepsilon(k)}{e^{[\varepsilon(k)-\mu]/T} \pm 1}. \quad (25)$$

In the Boltzmann limit and by taking into consideration just one resonance particle and its anti-particle, we get the expression given in Eq. (15). It is obvious that the trigonometric function included in the above expression are not truncated. In calculating this thermodynamic quantity, we sum up over all the hadron resonances we take into account.

We first start with two flavors. Here, it is not needed to care about the strangeness chemical potential. As discussed above, there are two lattice QCD simulations for $n_f = 2$. In the first one, re-weighting method is applied [4]. The physical quantities which usually can be calculated at $\mu_B = 0$ without any difficulties have responses at finite μ_B . The responses are utilized to estimate the thermodynamic quantities at finite μ_B . The other lattice simulations [3] use imaginary μ_B and afterwards apply analytical continuation. Some details about these simulations are given above. More details will be given below.

The masses of the non-strange hadron resonances in HRGM have to be re-scaled to heavy masses corresponding to the quark masses used in the lattice calculations. As mentioned above, the critical energy density is $\epsilon_c = 600 \text{ MeV/fm}^3$. At different μ -values, T_c is determined and defined as the temperature at which HRGM energy density reaches the value 600 MeV/fm^3 .

The results are plotted in Fig. 3. The solid circles represent the results for the *re-scaled* hadron resonance masses. These masses are comparable to the quark masses used in the lattice QCD simulations reported in Ref. [4]. The open circles represent the results for the physical masses. The two lines connecting the points are obtained by corresponding fit according to the following parabola:

$$\frac{T_c(\mu_q)}{T_c(\mu_q = 0)} = 1 - c_1 \left(\frac{\mu_q}{T_c(\mu_q = 0)} \right)^2. \quad (26)$$

The μ -values are restricted within the range $0 \leq \mu_q \leq T_c$. μ_q is given in Eq. (6). For the re-scaled heavy masses, the fit parameters are $c_1 = 0.115(36)$ and $T_c(\mu = 0) = 196.3 \text{ MeV}$. Plugging these parameters in Eq. (26), we get the top line in Fig. 3. The comparison with the lattice QCD calculations, Eq. (20), gives a satisfactory agreement, especially at low μ . Nevertheless, it is obvious that our points at large μ lie below the lattice results. The reason for this discrepancy will be discussed and handled later.

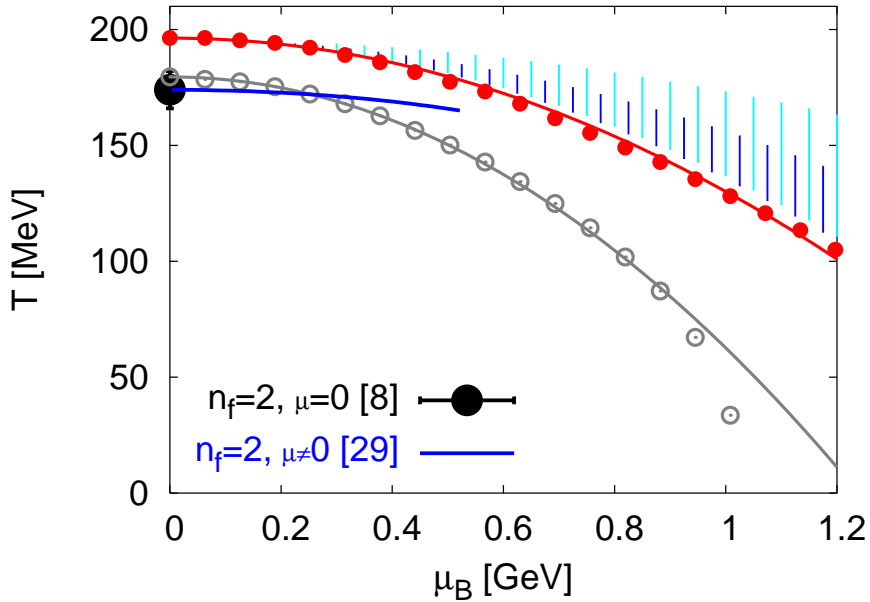


Fig. 3: The $T - \mu_B$ phase diagram for two quark flavors $n_f = 2$. The vertical lines give the lattice results [4]. The short lines show the results according to a constant energy density. The long ones are for constant critical temperature. The Lattice simulations are performed for large quark mass. The corresponding Goldstone pion gets a mass of 770 MeV. The solid circles give our results heavy quark masses. The results for physical quark masses are given by the open circles.

As given above, the coefficient given in the front of the term $(\mu_q/T)^2$ in Eq. (18) can be calculated. For non-strange hadron resonances with the re-scaled heavy masses, the coefficient gets the value 0.0767. Comparing to Eq. (20), this value is obviously much better than the value of c_1 in describing the lattice results. As we will see, this discrepancy comes from the fact that c_1 is calculated from fitting T_c for finite μ in the results obtained from non-truncated $\epsilon(T, \mu)$. Here, it should be emphasized that all Taylor terms higher than the second one are explicitly excluded in deriving Eq. (18). This partially explains the disagreement between HRGM and lattice results shown so far. As mentioned above, we also study the case of physical resonance masses. The fit parameters are $c_1 = 0.195(21)$ and $T_c(\mu = 0) = 175$ MeV. The coefficient in Eq. (18) is found to be 0.1368.

We can so far summarize that the curvature increases with reducing the quark masses. This might sound different that the lattice results that the curvature for two flavors is independent of the quark masses. The reason is that in the lattice calculations one has to apply different approximations in determining T_c , Eq. (19), especially for light quark masses.

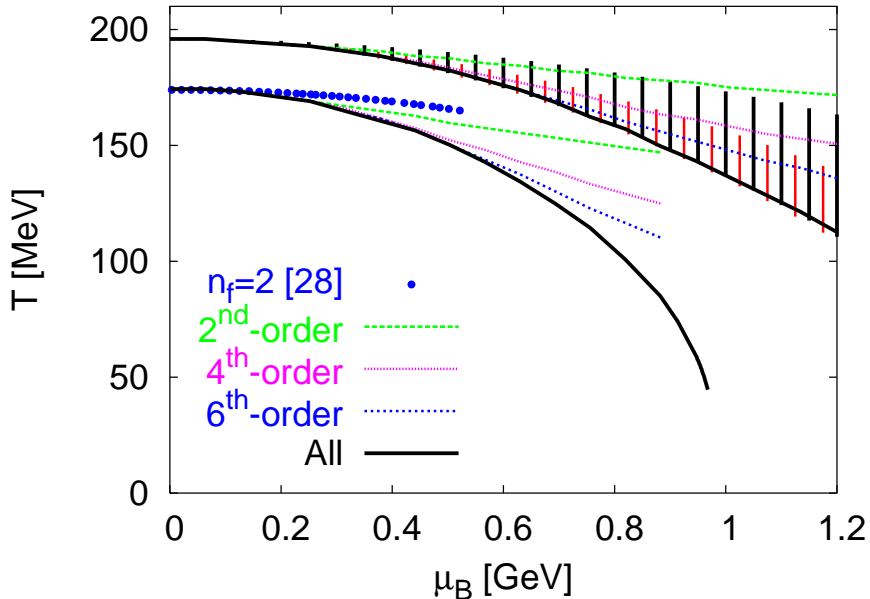


Fig. 4: The same as in Fig. 3. Here, we show the results obtained from the condition of constant energy density truncated up the different Taylor orders. The truncation is obviously able to describe the lattice QCD simulations for different quark masses [4, 29]. The solid lines give our predictions for non-truncated trigonometric functions.

In the following, we confront the lattice results with the HRGM results obtained from truncated expressions. In Fig. 4, we show the results obtained from the energy density with truncated trigonometric function. The truncation is done up to different orders. First, we start with the results obtained from the entire Taylor series of the trigonometric function for the re-scaled resonance masses. The solid line shows these results. This is equivalent to utilize Eq. (15) instead of Eq. (25). We note that this line shows almost the same behavior as that of the solid circles in Fig. 3. In deriving Eq. (15), the Boltzmann limit is assumed. The results from different truncations are also plotted. We find that the energy density truncated up to the second or forth order of μ/T is much better able to describe the lattice results than that from which the solid line has been obtained. The agreement between the curvatures of these two lines and that from the analytical expression Eq. (18) is excellent. The ability of the truncated expression of energy density to produce results comparable to the lattice ones is to be explained by the fact that the lattice results themselves have been obtained from a truncation up the the second order.

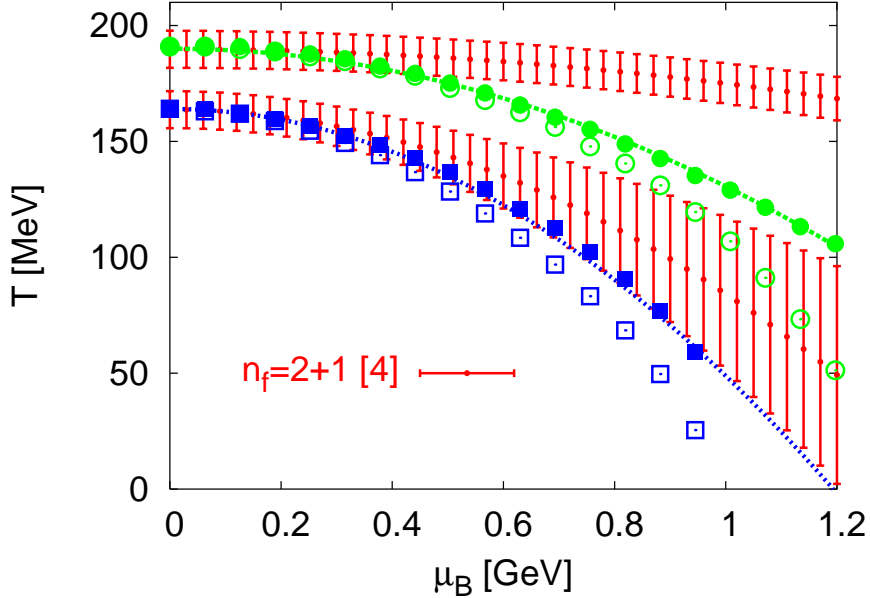


Fig. 5: The $T - \mu_B$ phase diagram for $n_f = 3$. The vertical short lines represent the lattice results [4]. The above band corresponds to heavy quark masses. The bottom one is for physical masses. The solid circles are our results for heavy resonances and for $\mu_s = 0$. The open circles are for $\mu_s = f(\mu_B, T)$. The squares give the results for the physical masses. The curves are fitted according to Eq. (26).

We draw in the same figure the results from the hadron resonances with the physical masses. The curves obtained from different truncation terms in Eq. (15) represent our predictions when the lattice simulations will be able to be performed at the physical mass. We note that the solid line is comparable to the bottom points plotted in Fig. 3. The quark masses used in Ref. [29] are relative heavy. Nevertheless, we see that the second order (dashed line) agrees very well with these lattice results [29] (solid circles).

B. Results for three flavors

We include the strange and non-strange hadron resonances with masses up to 2 GeV. We therefore have to deal with the strangeness chemical potential μ_s (Sec. II A). Assuming that the three quarks are degenerate, we can use the same critical energy density value as done in the previous section. The results are shown in Fig. 5. The solid circles show the results for the re-scaled resonance masses. As done in lattice calculations, we first ignore the change in μ_s . The resulting points (solid circles) are fitted within the range $0 \leq \mu_q \leq T_c$ according

to the parabola given in Eq. (26). The fit parameters are $T_c = 190$ MeV and $c_1 = 0.1016$. The coefficient in front of $(\mu/T)^2$ in Eq. (18) is 0.0505. Comparing with Eq. (22), this value can describe the lattice curvature better than c_1 . We also calculate μ_s at each μ and T assuming strangeness conservation. The open circles show these results. We note that the former case ($\mu_s = 0$) is much closer to the lattice results than the latter one. The reason is, as mentioned above, that μ_s is used to be set equals to zero in lattice QCD calculations.

The results for physical masses are also shown in Fig. 5. The solid squares represent the results at $\mu_s = 0$. These points are fitted according Eq. (26). The fit parameters are $T_c = 164$ MeV and $c_1 = 0.17$. The coefficient in the front of $(\mu/T)^2$ in Eq. (18) takes the value 0.1122, which agrees very well with Eq. (23). The open squares represent the results at varying μ_s . The results with re-scaled hadron masses are given as circles. The same conclusion as that for the re-scaled masses can be drawn here. With $\mu_s = 0$, we get results closer to lattice results than with $\mu_s = f(T, \mu_B)$.

In the this figure, the energy density is calculated according to Eq. (25). In other words, even if the energy density is given in the Boltzmann limit, the results plotted in this figure are deduced from expression like Eq. (15) without any truncations in its trigonometric function.

As done in the two flavor comparison, we plot in Fig. 6 the results obtained by applying different truncations. With this method, we can reliably compare our results with the lattice simulations. For re-scaled hadron masses, the results are given in the top panel. The results for physical masses are given in the bottom panel. It is clear that the truncation up to the second order gives results in a good agreement with the lattice simulations [4]. With higher truncation terms, we get curves with curvatures steady get larger than the lattice one. The curve obtained by using non-truncated expression of the energy density is also drawn. The solid curve is obtained by computing μ_s in dependence on both T and μ_B . Obviously, it is identical to the solid symbols plotted in Fig. 5. The dashed curve - next to the solid one - shows the results in which μ_s is entirely vanishing. It in turn shows the same behavior as that of the open symbols in Fig. 5. The same can be said about the results plotted in the bottom panel.

We can so far conclude that the lattice results [4] can very well be reproduced by HRGM, if the trigonometric function is truncated up to some Taylor terms. Concretely, the lattice

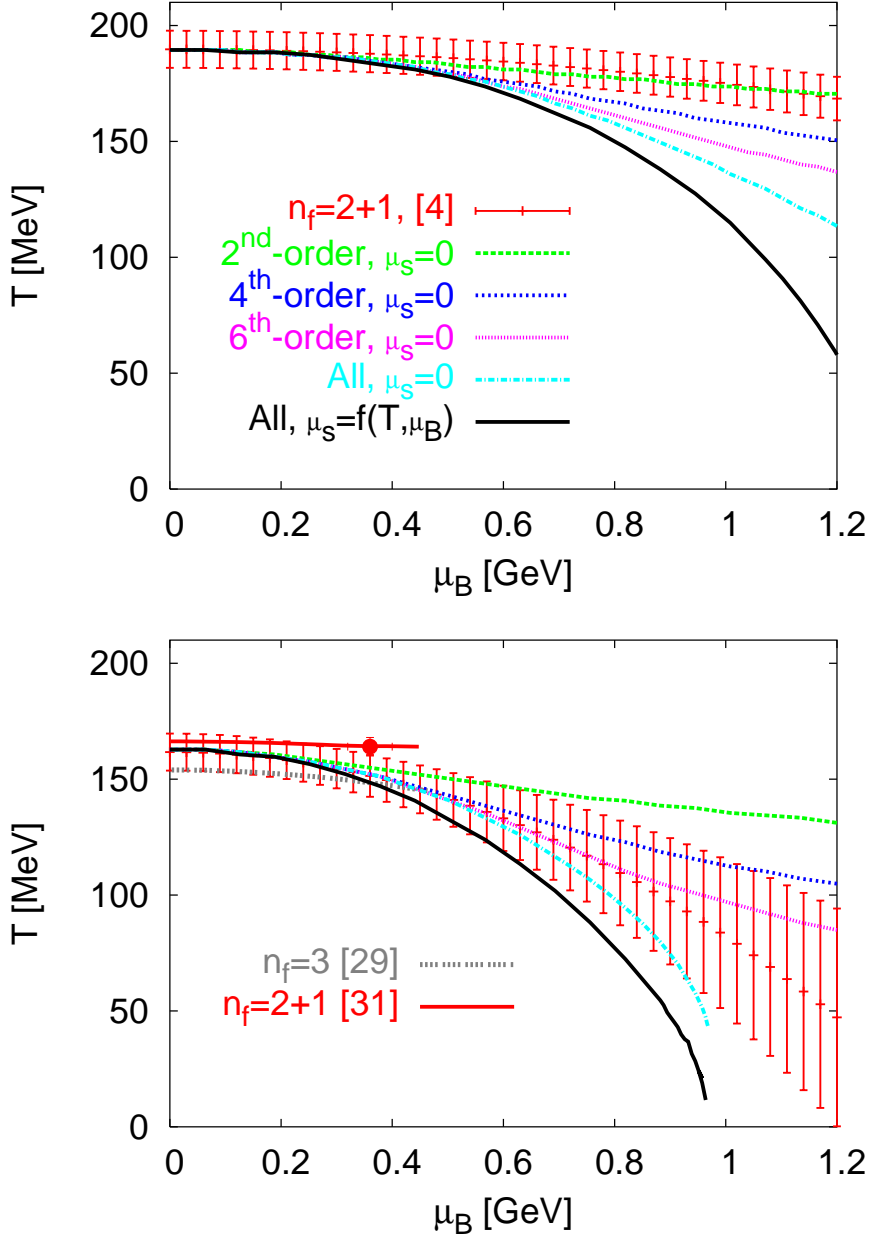


Fig. 6: $T - \mu_B$ phase diagram as in Fig. 5. Here, we check the effects of truncated trigonometric functions.

The top panel shows the results for heavy masses. Truncating $\epsilon(T, \mu_B)$ up to second order reproduces the lattice results [4]. In the bottom panel we show the results with physical masses. the lattice results [4] are very well reproduced by the condition of truncating ϵ . The results from non-truncated ϵ at $\mu_s = 0$ and $\mu_s = f(T, \mu_B)$ are also plotted. The agreement with the lattice simulations [29, 31] is also convincing

curvature within the region $0 \leq \mu_q \leq T_c$ can be very well described by HRGM, in which the expression for energy density is truncated up to the 2^{nd} or 4^{th} -term.

In the bottom panel, we also show other three flavor lattice results. In Ref. [29], the numerical simulations have been performed with Wilson gauge action and three degenerate flavors of staggered fermions. The quark masses are ranging between $0.025 \leq am_q \leq 0.04$. It is clear that our results agree well with these data. We see that the curvature can be described by our second or fourth order results. This is also valid for the lattice results for $n_f = 2 + 1$ which are reported in Ref. [31]. In this case, the lattice simulations are performed by using $am_{u,d} = 0.0092$ and $am_s = 0.25$. The chiral extrapolations are done by means of heavier light quark masses. The agreement with our results is obvious.

We also plot the latest calculations of the location of the endpoint. The endpoint in [32] lies at $\mu_B = 420$ MeV. The corresponding temperature has not yet been calculated. The endpoint in [31] has the coordinates $\mu_B = 360 \pm 40$ MeV and $T = 162 \pm 2$ MeV. As we discussed above, we assume that the existence of the endpoint does not affect the results reported here.

VI. RADIUS OF CONVERGENCE

In this section, we estimate the radius of convergence from the Taylor series. As we have seen, for a reliable comparison with the current lattice simulations, we have to apply truncations in the thermodynamic expressions in HRGM. Our objective here is to check the efficiency of the truncated series in locating the phase diagram. The radius of convergence can reflect the singularity near T_c . It approaches unity near T_c . We compare the results on different radii of convergence from HRGM and lattice [32].

As done in Ref. [21] and in Sec. III, the energy density normalized to T^4 can be expressed as a trigonometric function depending on the ratio μ/T . We also use the property that the energy density is an even function in μ_B/T and therefore write

$$\frac{\epsilon(T, \mu_B)}{T^4} = \epsilon_m(T) + \epsilon_b(T) \cosh\left(\frac{\mu_B}{T}\right) \approx \epsilon_b(T) \left[c_2 \left(\frac{\mu_q}{T}\right)^2 + c_4 \left(\frac{\mu_q}{T}\right)^4 \dots \right], \quad (27)$$

where $c_n = (T_c/T)^n 3^n/n!$ and n is an even positive integer. The radius of convergence is

$$\rho = \lim_{n \rightarrow \infty} \left| \frac{c_n}{c_{n+2}} \right|^{1/2}. \quad (28)$$

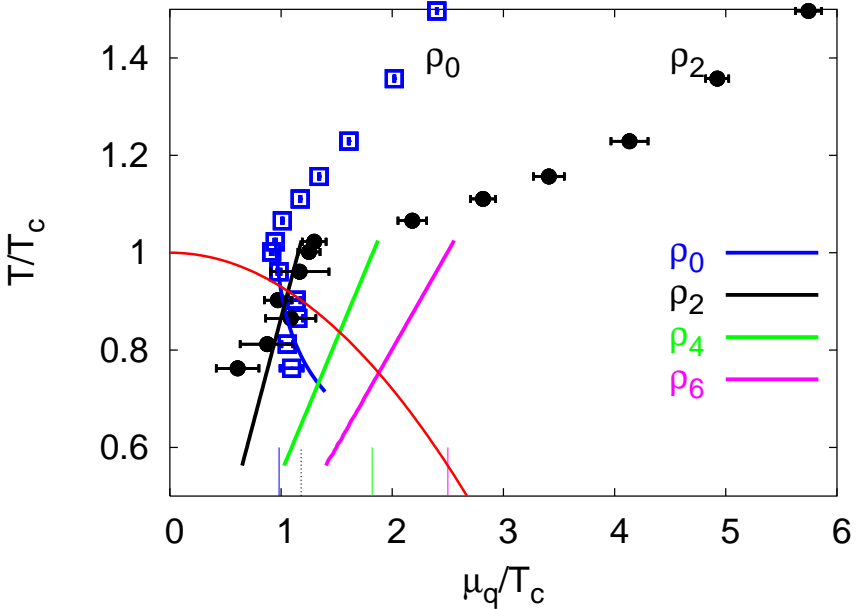


Fig. 7: Comparison between radii of convergence from the lattice [32] (points) and HRGM (lines). There is an excellent agreement with the existing lattice results. The T_c -curvature has been calculated by using lattice results with two flavors (Fig. 3). The short vertical lines give the values of corresponding radii at T_c .

In order to calculate the zero order radius, we need to recall the results at $\mu = 0$. This is not included in Eq. (27).

$$\rho_0 = \left(\frac{c_0}{c_2} \right)^{1/2} = \frac{T}{T_c} \left[\frac{2}{9} \left(\frac{\epsilon_m(T)}{\epsilon_b(T, \mu_q = 0)} + 1 \right) \right]^{1/2}. \quad (29)$$

It is clear that this radius of convergence strongly depends on T . In Fig. 7, we note that near T_c , $\rho_0 = 0.982$, $\rho_2 = 1.18$, $\rho_4 = 1.82$ and $\rho_6 = 2.5$. These values are shown as short vertical lines in Fig. 7. The results agree very well with the available lattice results. As given in Ref. [32], as $\rho_0 \rightarrow 1$, the radius of convergence approximately gives the lower bound for the critical endpoint ($\mu_q \geq T_c$). This value exceeds the recent lattice results [26, 31]. In principle, one expects that due to the absence of critical behavior in HRGM, the Taylor expansion Eq. (27) has an infinite convergence radius for all temperatures. At T_c , the degrees of freedom in the hadron matter get indistinguishable from those in QGP. In lattice QCD simulations, the radii ρ are bounded from above by the location of the phase transition line. Therefore, it is expected that the radii in Eq. (28) stay close to unity for temperatures close to T_c . In fact, this is the case for the low order expansion coefficients in HRGM. The agreement between our results and the lattice ones is excellent. There are no published

lattice results on the 6th-order radius of divergence. Nevertheless, according to our expansion coefficients, ρ are steadily changing.

VII. CONCLUSIONS

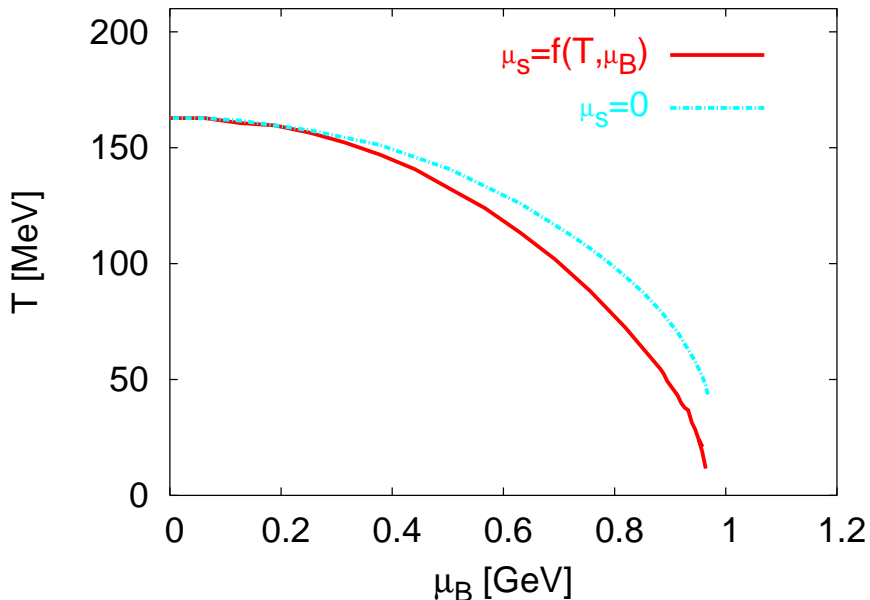


Fig. 8: Summary of our results on the QCD phase transition. In calculating both curves, we use all hadron resonances and suppose that the isospin chemical potential is vanishing. To obtain the top curve, we assigned μ_s to zero. μ_s is calculated in dependence on T and μ_B . The results are given by the bottom curve. We note that both curves will cross the abscissa at the point of normal nuclear density.

We have used the hadron resonance gas model (HRGM) to draw up the $T_c - \mu_B$ phase diagram. The transition temperature T_c from hadronic matter to QGP has been determined according to a condition of constant critical energy density. Its value is taken from lattice QCD simulations at zero chemical potential [8] and assumed to remain constant along the entire μ -axis. We checked the influence of the strangeness quark chemical potential μ_s on T_c . For including μ_s , we applied two models. In the first one, we have explicitly calculated μ_s in dependence on both T and μ_B . The condition is that the net strangeness particle density vanishes. In the second one, we assigned, as the case in lattice QCD simulations, zero to μ_s for all temperatures and baryo-chemical potentials μ_B . The first case, $\mu_s = f(T, \mu_B)$, is of great interest for heavy-ion experiments. Furthermore, under this consideration, the

strange quantum number is entirely conserved. This is not the case in the second model. Nevertheless, under the last assignment, the current lattice results are very well reproduced. On the other hand, one can apply the second model in high energy heavy-ion experiments. At BNL-RHIC and CERN-LHC energies, for instance, μ_B (and consequently μ_s) is very small. In the lattice QCD simulations, the calculations are used to be performed at $\mu_s = 0$. We have shown that the proper condition to guarantee vanishing strangeness in QGP is to set $\mu_s = \mu_q$. We did not check this explicitly. But it is obvious that $T_c(\mu_B, \mu_s = 0)$ quantitatively is not very much different from $T_c(\mu_B, \mu_s(T, \mu_B))$ at small chemical potentials.

We have taken into consideration all hadron resonances given in the particle data booklet with masses up to 2 GeV. For a reliable comparison, we have re-scaled the hadron masses to be comparable to the quark masses used in lattice simulations. By excluding the strange resonances, we can compare our results with the two flavor lattice results. By including all resonances, we have reproduced the three flavor lattice results. We note that increasing the chemical potentials μ_B and μ_s leads to a monotonic decrease in T_c . The results from HRGM match very well with the lattice simulations, especially within the μ -range in which the lattice calculations are most reliable ($\mu_q/T = \mathcal{O}(1)$). The agreement turns to be excellent, when we take into consideration the truncations done in calculating the thermodynamical quantity ϵ on the lattice in HRGM.

Besides this excellent agreement in the indirectly calculated T_c - via constant energy density - we find that the analytical expression of $T_c(\mu)$ up to the second order of the ratio $(\mu/T)^2$ greatly reproduces the curvatures calculated on the lattice for different masses and flavor numbers.

Fig. 8 summarizes our conclusions. The QCD phase diagram is plotted for a system contains strange and light quarks. In this figure, the Taylor series of the energy density is entirely taken into consideration. The curves represents our predictions, when it will be possible to perform lattice regularized QCD with physical masses and without truncating the Taylor series. As $T \rightarrow 0$, we note that both curves will cross the abscissa at almost one point. It is obvious that this point is corresponding to the normal nuclear density. The latter is related to $\mu_B \sim 0.979$ GeV. The nature of the phase transition at $T = 0$ does not lie within the scope of this work. However, there are many indications that the transition at $T = 0$ occurs according to modification in the particle correlations. Changing the correlation leads to quantum phenomena, like quantum entropy [13–18]. We also note that by switching on

μ_s an increase in T_c is expected. At small μ_B , the two curves are coincide.

Acknowledgments

We gratefully acknowledge the useful discussions with David Blaschke, Frithjof Karsch, Berndt Müller and Boris Tomasik.

[1] K. Rajagopal and F. Wilczek (2000), hep-ph/0011333.

[2] Z. Fodor and S. D. Katz, Phys. Lett. **B534**, 87 (2002), hep-lat/0104001.

[3] P. de Forcrand and O. Philipsen, Nucl. Phys. **B642**, 290 (2002), hep-lat/0205016.

[4] C. R. Allton et al., Phys. Rev. **D66**, 074507 (2002), hep-lat/0204010.

[5] M. D'Elia and M.-P. Lombardo, Phys. Rev. **D67**, 014505 (2003), hep-lat/0209146.

[6] R. V. Gavai and S. Gupta, Phys. Rev. **D68**, 034506 (2003), hep-lat/0303013.

[7] F. Karsch, Lect. Notes Phys. **583**, 209 (2002), hep-lat/0106019.

[8] F. Karsch, E. Laermann, and A. Peikert, Nucl. Phys. **B605**, 579 (2001), hep-lat/0012023.

[9] K.-F. Liu, Int. J. Mod. Phys. **B16**, 2017 (2002), hep-lat/0202026.

[10] A. Alexandru, M. Faber, I. Horvath, and K.-F. Liu (2004), hep-lat/0410002.

[11] A. Tawfik (2004), hep-ph/0410282.

[12] A. Tawfik (2004), hep-ph/0410392.

[13] D. E. Miller and A. Tawfik (2003), hep-ph/0308192.

[14] D. E. Miller and A. Tawfik (2003), hep-ph/0309139.

[15] D. E. Miller and A. Tawfik (2003), hep-ph/0312368.

[16] D. E. Miller and A. Tawfik, J. Phys. **G30**, 731 (2004), hep-ph/0402296.

[17] S. Hamieh and A. Tawfik (2004), hep-ph/0404246.

[18] D. E. Miller and A. Tawfik, Acta Phys. Polon. **B35**, 2165 (2004), hep-ph/0405175.

[19] F. Karsch, K. Redlich, and A. Tawfik, Phys. Lett. **B571**, 67 (2003), hep-ph/0306208.

[20] F. Karsch, K. Redlich, and A. Tawfik, Eur. Phys. J. **C29**, 549 (2003), hep-ph/0303108.

[21] K. Redlich, F. Karsch, and A. Tawfik, J. Phys. **G30**, S1271 (2004), nucl-th/0404009.

[22] D. Toublan and J. B. Kogut (2004), hep-ph/0409310.

[23] R. Hagedorn, Nuovo Cim. Suppl. **3**, 147 (1965).

- [24] R. Dashen, S.-k. Ma, and H. J. Bernstein, Phys. Rev. **187**, 345 (1969).
- [25] F. Karsch, Prog. Theor. Phys. Suppl. **153**, 106 (2004), hep-lat/0401031.
- [26] S. Ejiri et al., Prog. Theor. Phys. Suppl. **153**, 118 (2004), hep-lat/0312006.
- [27] A. Ali Khan et al. (CP-PACS), Phys. Rev. **D64**, 074510 (2001), hep-lat/0103028.
- [28] F. Karsch et al., Nucl. Phys. Proc. Suppl. **129**, 614 (2004), hep-lat/0309116.
- [29] P. de Forcrand and O. Philipsen, Nucl. Phys. **B673**, 170 (2003), hep-lat/0307020.
- [30] Z. Fodor, Nucl. Phys. **A715**, 319 (2003), hep-lat/0209101.
- [31] Z. Fodor and S. D. Katz, JHEP **04**, 050 (2004), hep-lat/0402006.
- [32] C. R. Allton et al., Phys. Rev. **D68**, 014507 (2003), hep-lat/0305007.
- [33] To clarify the dependence on the quark mass, we compare the full QCD with the pure gauge results. The values of ϵ_c/T^4 are different. But taking into consideration the different T_c -value, we find that the ϵ_c are comparable with each other.